INTERNATIONAL JOURNAL OF INTEGRATED ENGINEERING
ISSN: 2229-838X e-ISSN: 2600-7916

IJIE

Vol. 17 No. 5 (2025) 87-97
https://publisher.uthm.edu.my/ojs/index.php/ijie

Pore Characterization and Mechanical Properties of Triply Periodic Minimal Surfaces Porous Structures by Fused Deposition Modelling

Heng Liang Fan, Abdullah Yassin[1]*, Khairul Fikri Tamrin[1], Sinin Hamdan[1]

[1] *Faculty of Engineering,*
Universiti Malaysia Sarawak (UNIMAS), 94300 Kota Samarahan, Sarawak, MALAYSIA

*Corresponding Author: yabdulla@unimas.my
DOI: https://doi.org/10.30880/ijie.2025.17.05.008

Article Info

Received: 22 July 2024
Accepted: 6 March 2025
Available online: 30 August 2025

Keywords

Fused deposition modelling,triply periodic minimal surfaces, mechanical properties,energy absorption

Abstract

This paper focuses on the design and characterization of porous structures inspired by Triply Periodic Minimal Surfaces (TPMS) in the context of additive manufacturing. Uniform porous structures with porosities of 40% (P40), 50% (P50), and 60% (P60) are designed, along with a gradient porous structure with an average porosity of 50% (ZP50). Fused Deposition Modelling (FDM) serves as the fabrication method for these TPMS-based structures. The printing accuracy, mechanical properties and energy absorption characteristics of the TPMS porous structures with different porosity are investigated. A comprehensive evaluation reveals that the actual porosity deviates from the designed values by less than 4%, affirming the reliability of the design approach. Notably, an increase in porosity correlates with an increase in ultimate yield strength, reaching a peak value of 8.644 MPa for P40. Additionally, ZP50 shows a 15.54% higher yield strength than P50 under similar porosity conditions. This advantage persists up to a strain level of 26%, where ZP50 also outperforms P50 in energy absorption characteristics. The findings enrich the understanding of the mechanical behaviour of small-scale curved porous structures created through additive manufacturing. The research offers valuable insights for engineering applications that require optimized porous structures, thereby contributing to advancements in the additive manufacturing field.

1. Introduction

Triply periodic minimal surfaces (TPMS) are surfaces with zero curvature at any point and varying periodically in space. TPMS structures of various shapes can be obtained by controlling the relevant parameters of different types of implicit functions [1].TPMS porous structures have structural characteristics such as small unit density, high specific surface area and light weight, and functionally can achieve excellent load-bearing capacity [2], energy absorption properties [3] , thermal conductivity and biocompatibility [4], and have wide application prospects in many fields such as aerospace, mechanical electronics and biomedicine [5-7].

Traditionally, the preparation accuracy of TPMS structures is difficult to control, but with the rapid development of additive manufacturing technology, the problem of difficult preparation of TPMS structures has been basically solved. It has also promoted the research on the design as well as the performance of TPMS structures by domestic and foreign scholars [8-9]. Sharma et al. [10] reviewed the design, fabrication, and performance of triply periodic minimal surface-based mechanical metamaterials produced by additive manufacturing, highlighting their structural advantages, application challenges, and future prospects. Kumar et al.

This is an open access article under the CC BY-NC-SA 4.0 license.

[11] designed and parameterized TPMS lattice structures using a combined computational and experimental approach, and systematically evaluated their mechanical performance. Qiu et al. [12] designed three-dimensional functionally graded triply periodic minimal surface structures and systematically investigated their mechanical properties under different loading conditions. Sun et al. [13] analyzed the compression properties of the molded structures based on the design of TPMS structures by selective laser melting (SLM). The morphology of the TPMS structure was observed and the defects of the porous structure prepared by SLM were analyzed. The results showed that the compressive mechanical properties of different cellular structures are governed by the relative density. The cell geometry and the sheet-based Ti6Al4V alloy TPMS structures achieve excellent energy absorption capacity, which can be attributed to the smooth interconnected curved surfaces of the sheet-based TPMS structure and optimized process parameters. Al-Ketan et al. [14] investigated cellular steel solids with shell-like periodic architectures fabricated by selective laser sintering and systematically analyzed their mechanical properties and energy absorption performance. Alizadeh et al. [15] prepared Gyroid polylactic acid (PLA) scaffolds by fused deposition modeling and obtained the compressive elastic modulus and yield strength of the scaffolds. The results showed that both the dense PLA and porous PLA scaffolds showed elastic-plastic deformation behavior in both building and transverse directions. Cecen et al. [16] used fused deposition modeling technology to design and fabricate polylactide (PLA)/polyhydroxyalkanoate (PHA) scaffolds with specific porosity. The mechanical properties of lattices based on triple periodic minimal surfaces (TPMS) were investigated. The results indicated that enhanced pore size control can be achieved by 3D printing techniques. Peng et al. [17] designed and prepared two types of triple periodic minimal surfaces (TPMS) with homogeneous and gradient properties using fused deposition modeling (FDM). The effects of relative density and loading rate on the mechanical properties and deformation behavior of the structures were analyzed. In addition, the mechanical response characteristics and deformation modes of the gradient structures are not affected by the loading rate, while the uniform structures show significant softening behavior.

Despite some progress in current research on the design, preparation, and mechanical properties of uniform and gradient porous structures, there is a need for further investigation into the relationship between design parameters, pore characteristics, mechanical properties, and energy absorption capacity. In this study, uniform and gradient porous structures were designed with different levels of porosity based on the Primitive structure, which has demonstrated excellent fabrication performance in TPMS. These structures were fabricated using the fused deposition technique. The pore characteristics were examined using a Scanning Electron Microscope and the mechanical properties evaluated through compression testing. The objective is to uncover the influence of relevant structural parameters on the compression performance and energy absorption characteristics of TPMS porous structures. By doing so, this research aims to establish a design foundation for expanding the engineering applications of porous structures.

2. Porous Structure Design

2.1 Uniform Porous Structure Design

Modeling methods based on triply periodic minimal surface porous structures usually use implicit sinusoidal periodic functions for the approximate expression of TPMS surfaces by the following Equation [18]:

$$\varphi_{(r)} = \sum_1^k A_k \cos\left[2\pi(h_k r)/\delta_k + p_k\right] = T \tag{1}$$

where A_k is the amplitude factor, r is the position vector, h_k is the kth lattice vector in inverse space, δ_k is the wavelength of the period, p_k is the phase, and t is the threshold.

In order to obtain the TPMS structural model more accurately, the ideal structural model can be obtained by establishing different types of implicit expressions. In this paper, the Primitive structure with good fabrication properties is chosen [19-20], and the implicit expression of this structural model is given in the following Equation [21]:

$$\varphi_P = cos(\frac{2\pi}{L}x) + cos(\frac{2\pi}{L}y) + cos(\frac{2\pi}{L}z) - t = 0 \tag{2}$$

where L is the edge length of the TPMS single cell in the x, y, and z directions, mm. The subscript P refers to the abbreviation of Primitive structure. The implicit surface of the Primitive structure can be constructed by the triangular periodic functions in the x, y, and z directions in equation (2). The implicit surface polygonization algorithm is used to model the triply periodic minimal surface to obtain the CAD model of the Primitive porous structure, as shown in Fig. 1.

Int. Journal of Integrated Engineering Vol. 17 No. 5 (2025) p. 87-97

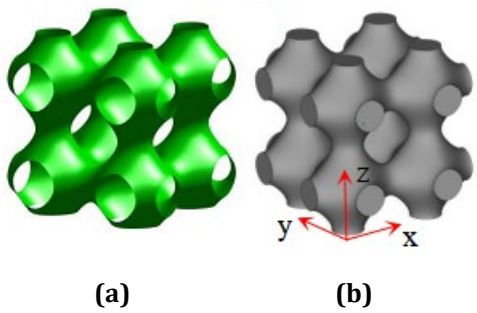

Fig. 1 *Primitive porous structure CAD model (a) Primitive minimum surface; (b) Primitive porous structure*

From equation (2), it can be seen that the internal porosity of the Primitive structure can be regulated by changing the magnitude of *t*. The relationship between the porosity *P* and *t* is fitted using Matlab software, and the fitting results are shown in Fig. 2. It can be seen that the relationship between *P* and *t* for the Primitive structure is linear and the value of the desired P corresponding to t can be obtained by the fitted function.

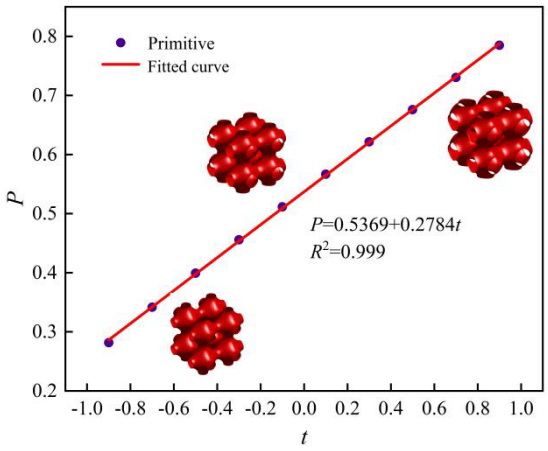

Fig. 2 *Relationship between porosity P and threshold t of Primitive porous structure*

2.2 Linear Gradient Porous Structure Design

In order to obtain the Primitive porous structure with a linear gradient, the linear porosity gradient equation of *t* versus z-axis is constructed using the implicit surface structure design method of the linear gradient, which is shown in equation (3). According to the required porosity, coefficients *a* and *b* can be derived by the method of coefficients to be determined, thus controlling the range of gradient variation of porosity.

$$\varphi_P = cos(\frac{2\pi}{L}x) + cos(\frac{2\pi}{L}y) + cos(\frac{2\pi}{L}z) - (a + b * z) = 0 \quad (3)$$

For a comprehensive comparison, set L = 3 mm and $0 \le x, y, z \le 32$ mm in Equations (2) and (3), and design a uniform Primitive porous structure with 40%, 50%, and 60% porosity, i.e., P40, P50, and P60, using equation (2). Design a uniform Primitive porous structure with an average porosity of 50% and a linear gradient along the z-axis using equation (3). Design a uniform Primitive porous structure with 60% and 40% porosity at the bottom and top of the gradient structure, i.e., ZP50. The designed model was materialized using Materialise Magics 22.0 software, and the X-Y plane schematic and solid models of different porous structures are shown in Table 1.

Table 1 *The X-Y plane schematic and solid model of the different porous structures*

Type	X-Y	Solid Model
(a) Uniform-40%（P40）	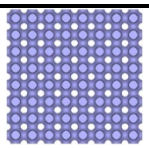	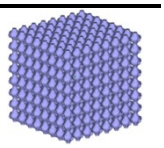
(b) Uniform-50%（P50）	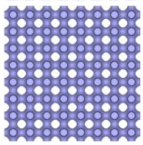	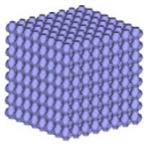
(c) Uniform-60%（P60）	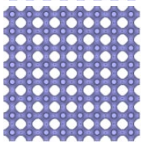	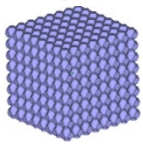
(d) Gradient-60%-40%（ZP50）	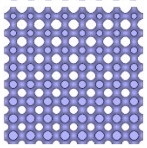	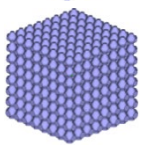

2.3 Materials and Methods

PLA Disc-shaped filament material, 1.75 mm in diameter was supplied by Beijing Taier Times Technology Co. The FDM 3D printer used was ET4, Shenzhen Aynet Technology Co., Ltd; The electronic analysis balance with precision 0.001 g, are from Qingdao Jingcheng Instrument Co., Ltd. The scanning electron microscope used was EVO-18, Carl Zeiss AG (Zeiss Group). The microcomputer-controlled electronic universal testing machine used are UTM6104, Shanghai Sanshi Machinery Manufacturing Co. The STL model of the porous structure was imported into the slicing software of the FDM machine for processing. Four porous structures, namely uniform porous structure: P40, P50, P60, and gradient porous structure: ZP50 as well as a solid block of the same volume, were molded using the Enable ET4 molding machine. The molding process parameters were kept constant, with a printing temperature of 210 ℃, a layer thickness of 0.2 mm, a scanning speed of 90 mm/s, and the other parameters use the factory defaults. The FDM molded porous structure samples can be seen in Fig.3.

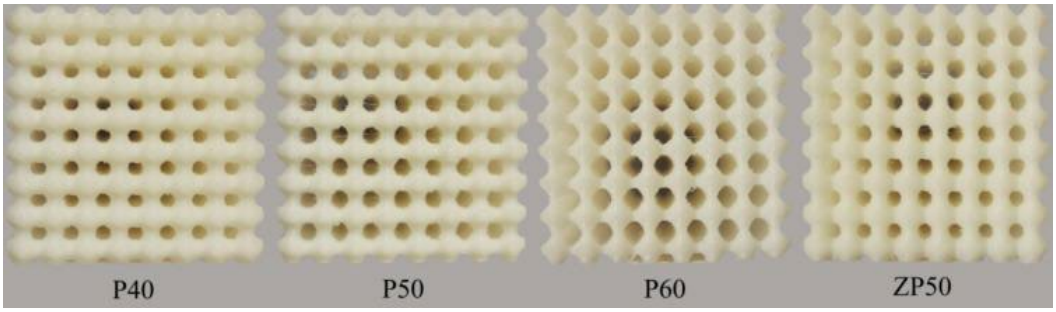

Fig. 3 *Porous structures samples fabricated by FDM*

The average porosity of porous structures was measured using the weighing method [22] with the Equation (4) :

$$\bar{P} = \left(\frac{m_1 - m_2}{m_1} \right) * 100\% \tag{4}$$

where m_1 is the mass of the solid structure with the same form factor as the porous structure, and m_2 is the mass of the porous structure after forming.

Based on the ASTM D1621 standard, uniaxial quasi-static compression tests were performed at 50 kN load at room temperature using the UTM6104 tester at 2 mm/min, with three specimens tested for each structure. The sample is placed in the centre of the platen as shown in Figure 4, ensuring that the pressure is transmitted in a vertical direction. A digital camera was used to record the compression process at a height parallel to the

Int. Journal of Integrated Engineering Vol. 17 No. 5 (2025) p. 87-97

specimen. The microcomputer system allows the acquisition of the displacement and pressure at the pressure at each moment, and the corresponding strain can be obtained based on the displacement of the indenter. According to the equivalent cross-sectional area of the porous structure and the pressure load, the corresponding stress data can be obtained, and finally obtain the corresponding stress-strain curve.

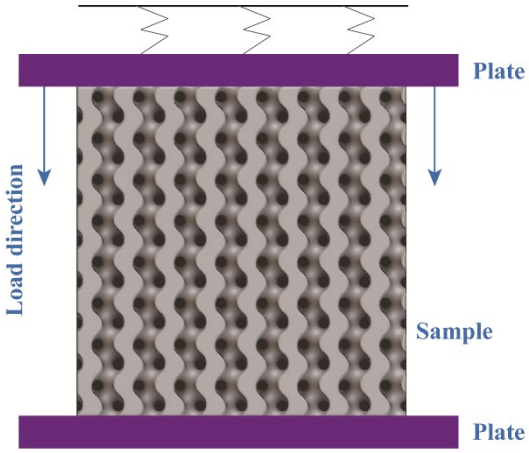

Fig. 4 *Schematic diagram of compressive test*

An EVO-18 scanning electron microscope (SEM) from Zeiss, Germany, was used to characterize the surface morphology as well as the rod diameter morphology of the samples, and the pore characteristics of the molded porous structures were analyzed based on the SEM images of the samples.

3. Results and Discussion

3.1 Pore Characterization

Each sample was weighed using an electronic analytical balance, and the average porosity of the porous structure was calculated according to equation (4). The designed porosity and actual measured porosity were compared, as shown in Fig. 5. The actual porosities of the measured samples are smaller than the designed values, and the deviations are between 1.5% and 4%. These deviations are caused by the precision of the 3D printer, unfused powder, and shrinkage during the molding process [23]. Notably, for the uniform structures, the deviation in actual porosity diminishes as the designed porosity (P) increases. Moreover, the ZP50 structure, characterized by its gradient variation, exhibited a slightly smaller deviation in actual porosity compared to the P50 structure with equivalent design porosity.

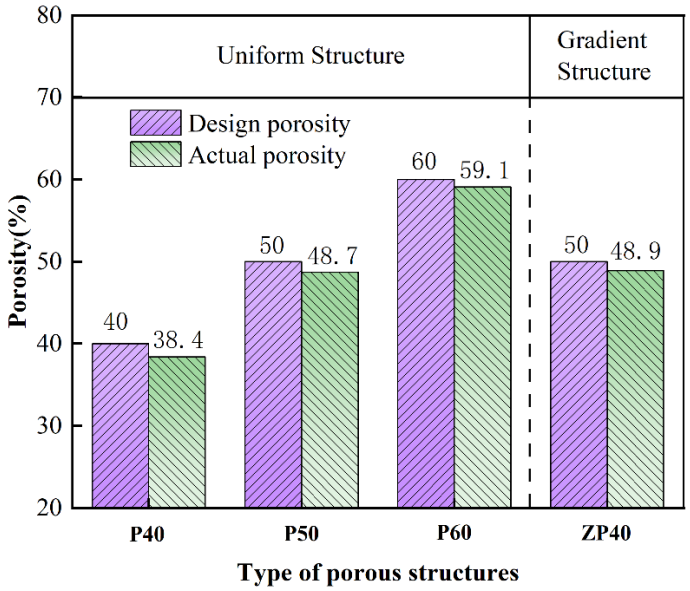

Fig. 5 *Comparison between the design and actual porosity of porous structures*

Macroscopic and microscopic features of the porous structure were meticulously analysed using both optical miscroscopy and Scanning Electron Microscopy (SEM), as illustrated in Fig. 6. Panels a1-d1 of Fig. 6 reveal the absence of material obstruction within the post-fabrication structure, confirming well-interconnected pores and overall structural integrity. This substantiates the feasibility of employing Fused Deposition Modelling (FDM) in the creation of Triply Periodic Minimal Surfaces (TPMS) porous structure, all of which exhibited seamless, defect-free surfaces. According to Equation (4), the empirically measured porosity for both uniform and gradient porous configurations was consistently lower than the design structure as corroborated by Fig. 4. This discrepancy is largely due to the adhesion of semi-fused material on the porous structure's surface, as depicted in Fig. 6, panels a3-d3, leading to a reduction in actual porosity.

As porosity increases, the structure's surface area diminishes, resulting in decreased adherence of unformed powder and, consequently, a reduction in porosity deviation. Elevated porosity levels also induce incomplete molding of certain support elements, adversely affecting the final product's quality, as evidenced in Fig. 6, panel c3. These findings align with those reported by Fan [24], indicating that some powder particles fail to achieve a fully molten state, thereby causing a minor deviation between actual and designed pore dimensions, as illustrated in Fig. 6, panels a2-d2.

For identical porosity levels, the ZP50 structure exhibits a lower deviation in porosity compared to the P50 structure. This is attributable to the gradient nature of the ZP50 configuration, which comprises a range of varying porosities (P40-P50-P60), as delineated in Table 1 (d).

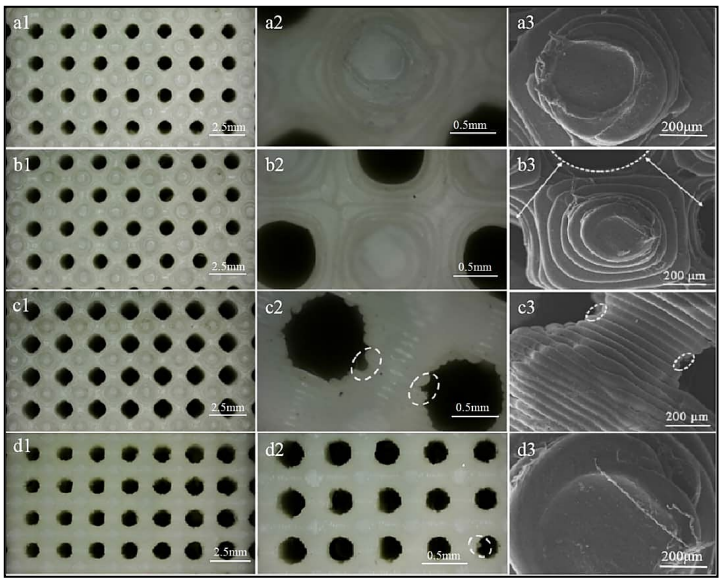

Fig. 6 *Macroscopic and microscopic morphology of porous structures (a1-a3) P40; (b1-b3) P50; (c1-c3) P60; (c1-c3) ZP50*

3.2 Compressive Performance

The compressive stress-strain curves for the uniform and gradient porous structures are depicted in Fig. 7. The yield strength values shown in Table 2 are obtained from Fig. 7. It can be seen that the yield strength of the uniform Primitive structure decreases with porosity, with the maximum yield strength of 8.644 MPa for the P40 structure and the minimum yield strength of 4.311 MPa for the P60 structure, see Table 2. This decrease in yield strength with increasing porosity is attributed to the reduction in wall thickness of the porous structure, consequently leading to lower modulus of elasticity and yield strength. This relationship between increased porosity and reduced yield strength is further validated by the work of Zhang et.al [25]. This study highlights the unique mechanical characteristics, such as yield strength, elastic modulus, and yield strength, of the gyroid-type TPMS lattice structures.

In relation to the effect of gradient porous structures on mechanical characteristics, the ZP50 structure shows a 15.54% higher yield strength than the P50. The ZP50 achieves a strength of 7.533 MPa, while the P50 reaches 6.362 MPa, as presented in Table 2. This difference in strength is attributed to the gradual variation in unit cell type and porosity in the ZP50 structure. This indicates the higher mechanical capabilities of the gradient porous structure. Such a combination of graded porosities and structures not only retains the characteristics of uniform structures but also highlights the distinct responses of the graded structures, aligning with findings in other research [26]. During compression, porous structures typically experience linear elastic deformation, leading to

Int. Journal of Integrated Engineering Vol. 17 No. 5 (2025) p. 87-97

yielding, and ultimately failure. Specifically, the ZP50 structure, with its gradient porous nature, displays a non-uniform stress and strain distribution. This is evident in Fig. 7b, where the plateau phase of the ZP50 curve shows more pronounced fluctuations and noticeable softening compared to P50. These fluctuations in ZP50 are attributed to structural weakening rather than strain rate variations.

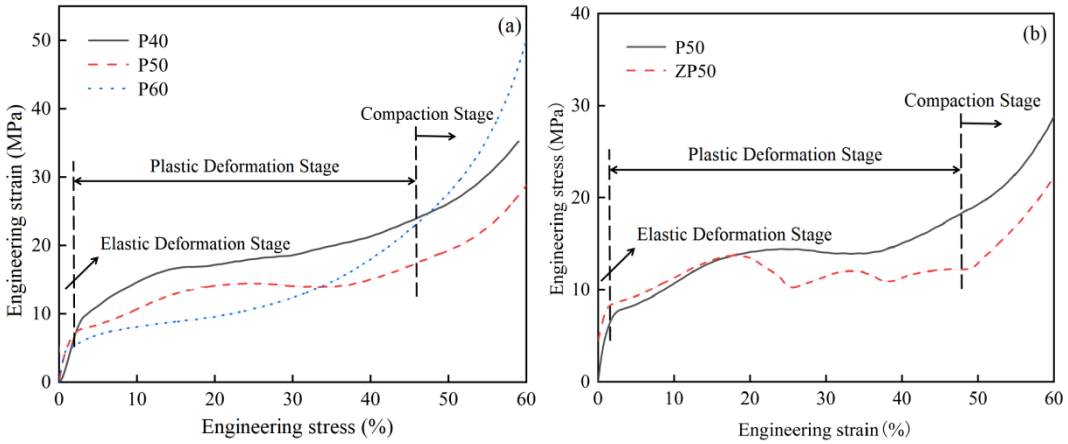

Fig. 7 *Compressive stress-strain curves (a) Uniform porous structure; (b) Uniform vs gradient porous structure*

Table 2 *Elastic modulus and yield strength of TPMS porous samples*

Type	Porosity (%)	Yield strength (MPa)	Elastic modulus (MPa)
Primitive	40	8.64±0.15	41.53±0.02
	50	6.36±0.13	33.82±0.07
	60	4.31±0.24	32.94±0.11
Z-Primitive	50	7.53±0.07	40.98±0.08

Fig. 8 in subchapter 3.2 and 3.3, we added fundamental reasons on occurrence of the phenomena, as follows: Fig. 8 shows the deformation behavior of the uniform and linear gradient porous structure during the compression process. It can be seen that the uniform porous structure is firstly damaged in the middle part during the compression process, and gradually barreling from the top and low end to the middle part until it is compacted, as shown in Fig. 8a. The middle layer of the porous structure undergoes initial yielding and gradually deforms at an inclination of approximately 45°. Eventually, it is completely crushed, as depicted in Fig. 8b. As mechanical compression proceeds, the uniform porous structure begins to produce layer-to-layer mutual compression. After passing through the elastic region plastic strain occurs and a deformation pattern of localized collapse occurs. Through continued compression, the collapse continues from layer to layer, eventually leading to overall fracture deformation. The gradient porous structure did not have uniform strength, so failures is not due to barreling, and it can happen at any layer of weakness. During the compressive deformation process, the designed porous structure changes in a linear gradient due to the linear gradient. The compressive stresses applied at each structural level are first released at the weakest pore structure of the scaffold, leading to the formation of relative slip between the inner layers of the porous structure. Under continuous application of compressive force, the porous structures with different strengths cracked one after another. The interlayer slip continues to extend to the porous scaffolds surrounding their pores. This eventually leads to complete fracture and collapse of all layers of the porous structure.

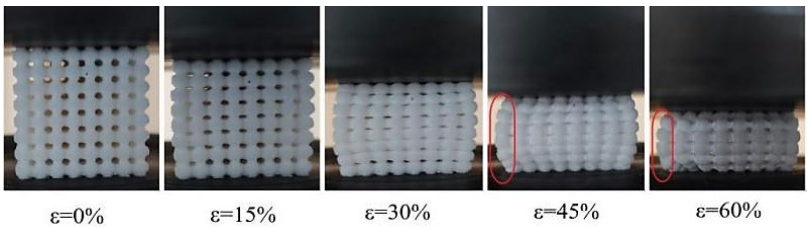

(a)

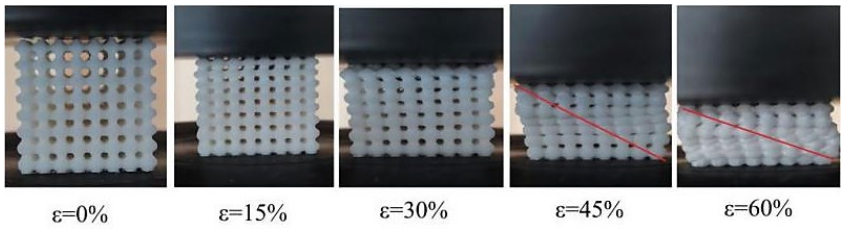

(b)

Fig. 8 *Deformation behavior of porous structures (a) Deformation behavior of uniform porous structures; (b) Deformation behavior of gradient porous structures*

3.3 Energy Absorption Characteristics

The properties of porous structures in terms of energy absorption are of great interest. It is one of the important indicators for the evaluation of porous structures [27]. The formula for calculating the total energy absorption per unit volume is shown in Equation (5).

$$W_\varepsilon = \int_0^\varepsilon \sigma(\varepsilon) d\varepsilon \tag{5}$$

where W_ε is the total energy absorption per unit volume, $\sigma(\varepsilon)$ is the pressure at strain ε, ε is the strain.

The stress-strain values of the porous structure and equation (4) are used to plot the curve of W_ε versus ε for the porous structure, as shown in Fig. 9. The larger the slope of the W_ε-ε curve, the better the energy absorption characteristics of the structure [28]. From Fig.8a, it can be seen that W_ε increases with strain ε. For the uniform porous structure, the slope of the W_ε-ε curve showed the magnitude of P40 > P50> P60. This indicates that the total energy absorption per unit volume, W_ε, decreases with porosity, which is in agreement with previous studies [29-30]. From Fig. 9b, the ZP50 structure has better energy absorption characteristics than P50 up to 26% ε under the same porosity. Above 26% ε, the energy absorption characteristics are weakened, which is attributed to the structural weakening in ZP50 as shown in Fig. 7b.

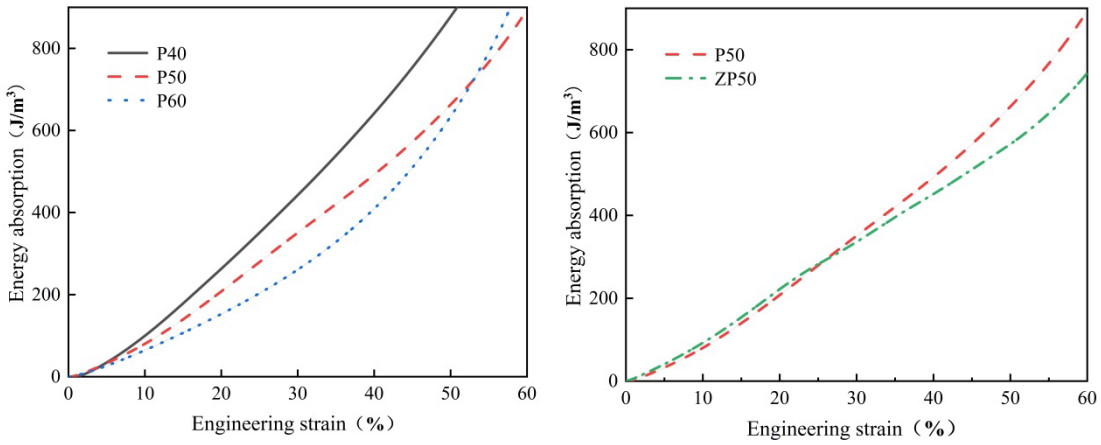

(a) **(b)**

Fig. 9 *Wε-ε curves of uniform and gradient porous structures (a) Wε-ε for P40, P50 & P60; (b) Wε-ε for P50 & ZP50*

4. Conclusion

(1) The uniform primitive porous structure was designed based on the triply periodic minimal surfaces, and the relationship between P and t of this structure was established. The porosity gradient equation was introduced to obtain a linear gradient porous structure model.

(2) The uniform and gradient porous structures with different porosity were printed and formed by the Fused Deposition Modelling (FDM) technique. The pores within the formed structure were well penetrated and the structure was basically uniform. The deviation in porosity between the designed and fabricated samples was less than 4%. This shows that using FDM for additive manufacturing is both cost-effective and promising when making TPMS porous structures.

(3) Different levels of porosities, 40%, 50% and 60%, influence the mechanical and energy absorption properties of the porous structure. The yield strength of the uniform Primitive porous structure decreases with porosity. This occurs because higher porosity leads to thinner walls in the structures, which reduces their elasticity and strength.

(4) Comparing uniform and gradient porous structures with the same porosity, the energy absorption efficiency of the gradient porous structure (ZP50) is 287 J/m3, which is slightly higher than uniform porous structure (P50) up to a strain of 26%. However, beyond this strain, the energy absorption of ZP50 becomes lower than that of P50.

Acknowledgement

We would like to acknowledge the support given by the Universiti Malaysia Sarawak towards this project. We also thank our colleagues and collaborators for their support and assistance throughout the research process.

Conflict of Interest

Authors declare that there is no conflict of interests regarding the publication of the paper.

Author Contribution

The authors are responsible for the study conception and design, data collection, analysis and interpretation of results, and manuscript preparation.

References

[1] Hu, X. Y., Min, X., Ricky, C. (2020). Piezoelectric properties of triply periodic minimum surface structures. *Composites Science and Technology*, 200, 108417, https://doi.org/10.1016/j.compscitech.2020.108417

[2] Ma, S., Tang, Q., Feng, Q. X. (2019). Mechanical behaviours and mass transport properties of bone-mimicking scaffolds consisted of gyroid structures manufactured using selective laser melting. *Journal of the Mechanical Behavior of Biomedical Materials*, 93, 158-169, https://doi.org/10.1016/j.jmbbm.2019.01.023

[3] Al-Saedi, D. S. J., Masosd, S. H., Mu, F. Z. (2018). Mechanical properties and energy absorption capability of functionally graded F2BCC lattice fabricated by SLM. *Material & Design*, 144, 32-44, https://doi.org/10.1016/j.matdes.2018.01.059

[4] Ma, S., Tang, Q., Han, X. X., Feng, Q. X. (2020). Manufacturability, Mechanical Properties, Mass-Transport Properties and Biocompatibility of Triply Periodic Minimal Surface (TPMS) Porous Scaffolds Fabricated by Selective Laser Melting. *Materials & Design*, 195, 109034, https://doi.org/10.1016/j.matdes.2020.109034

[5] D.M. Bragin, A.I. Popov, A.V. Eremin. (2024). The thermal conductivity properties of porous materials based on TPMS. *Chemical Industry and Engineering Progress*, 231, 125863, https://doi.org/10.1016/j.ijheatmasstransfer.2024.125863

[6] Liu, Z. Q., Gong, H., Gao, Z. J. (2021). Design of new gradient scaffolds based on triply periodic minimal surfaces and study on its mechanical, permeability and tissue differentiation characteristics. *Journal of Biomedical Engineering*, 38(5), 960-968, https://doi.org/10.7507/1001-5515.202102054

[7] Feng, J. W., Fu, J. Z., Yao, X. H. (2022). Triply periodic minimal surface (TPMS) porous structures: From multi-scale design, precise additive manufacturing to multidisciplinary applications. *International Journal of Extreme Manufacturing*, 4(2), 5-35, https://doi.org/10.1088/2631-7990/ac5be6

[8] Şimşek, U., Akbulut, A., Gayir, C. E., Basaran, C., Sendur, P. (2021). Modal characterization of additively manufactured TPMS structures: comparison between different modeling methods. *International Journal of Advanced Manufacturing Technology*, 115(23), 657–674, https://doi.org/10.1007/s00170-020-06174-0

[9] Wang, Z. G., Wang, X. X., Gao, T. Y. (2021). Mechanical behavior and deformation mechanism of triply periodic minimal surface sheet under compressive loading. *Mechanics of Advanced Materials and Structures*, 28(19), 2057-2069, https://doi.org/10.1080/15376494.2020.1829756

[10] Sharma, D., Hiremath, S. S. (2021). Additively manufactured mechanical metamaterials based on triply periodic minimal surfaces: Performance, challenges, and application. *Mechanics of Advanced Materials and Structures*, 29(26), 5077–5107, https://doi.org/10.1080/15376494.2021.1948151

[11] Kumar, R., Ramkumar, J., Balani, K. (2024). Design and parametrization of TPMS lattice using computational and experimental approach. *Engineering Research Express*, 6(3), 035556, https://doi.org/10.1088/2631-8695/ad7109

[12] Qiu, N., Zhang, J. Z., Li, C. Y., Shen, Y. J., Fang, J. G. (2023). Mechanical properties of three-dimensional functionally graded triply periodic minimal surface structures. *International Journal of Mechanical Sciences*, https://doi.org/10.1016/j.ijmecsci.2023.108118

[13] Sun, Q. D., Sun, J., Guo, K. (2022). Compressive mechanical properties and energy absorption characteristics of SLM fabricated Ti6Al4V triply periodic minimal surface cellular structures. *Mechanics of Materials*, 166, 104241, https://doi.org/10.1016/j.mechmat.2022.104241

[14] Al-Ketan, O., Rowshan, R., Palazotto, A. N., & Abu Al-Rub, R. K. (2019). On mechanical properties of cellular steel solids with shell-like periodic architectures fabricated by selective laser sintering. *Journal of Engineering Materials and Technology*, 141(2), 021009, https://doi.org/10.1115/1.4041874

[15] M. Alizadeh-Osgouei, Y. Li, A. Vahid, A. Ataee, C. Wen (2021). High strength porous PLA gyroid scaffolds manufactured via fused deposition modeling for tissue-engineering applications. *Smart Materials in Medicine*, 22021, 15-25, https://doi.org/10.1016/j.smaim.2020.10.003

[16] Cecen, B. (2021). FDM-based 3D printing of PLA/PHA composite polymers. *Chemical Papers*, 2023, 77:4379–4386, https://doi.org/10.1007/s11696-023-02786-4

[17] Feng, G., Li, S., Xiao, L. (2023). Mechanical properties and deformation behavior of functionally graded TPMS structures under static and dynamic loading. *International Journal of Impact Engineering*, 176, 104554, https://doi.org/10.1016/j.ijimpeng.2023.104554

[18] Abyeidda, D. W., Bakir, M., Abu R, K. (2017). Mechanical properties of 3D printed polymeric cellular materials with triply periodic minimal surface architectures. *Materials & Design*, 122, 255-267, https://doi.org/10.1016/j.matdes.2017.03.018

[19] Shevchenko, V., Balabanov, S. (2023). Prediction of Cellular Structure Mechanical Properties with the Geometry of Triply Periodic Minimal Surfaces (TPMS). *ACS Omega*, 8, 26895−26905, https://doi.org/10.1021/acsomega.3c01631

[20] Saleh, M., Anwar, S., Al-Ahmari, A. M., & Alfaify, A. (2023). Compression Performance and Failure Analysis of 3D-Printed Carbon Fiber/PLA Composite TPMS Lattice Structures. *Polymers*, 14(21), 4595. https://doi.org/10.3390/polym14214595

[21] Yoo, D. J. (2011). Computer-aided porous scaffold design for tissue engineering using triply periodic minimal surfaces. *International Journal of Precision Engineering and Manufacturing*, 12(1), 61-71, https://doi.org/10.1007/s12541-011-0008-9

[22] Khanna, P., Sood, S., Mishra, P., Singh, S. J. (2024). Analysis of compression and energy absorption behaviour of SLM printed AlSi10Mg triply periodic minimal surface lattice structures. *Structures,* 64, 106580, https://doi.org/10.1016/j.istruc.2024.106580

[23] Wang, N., Meenashisundaram, G. K., Chang, S. (2022). A comparative investigation on the mechanical properties and cytotoxicity of Cubic, Octet, and TPMS gyroid structures fabricated by selective laser melting of stainless steel 316L. *Journal of the Mechanical Behavior of Biomedical Materials*, 219, 105151, https://doi.org/10.1016/j.jmbbm.2022.105151

[24] Fan, X. J., Tang, Q., Feng, Q. X. (2021). Design, mechanical properties and energy absorption capability of graded-thickness triply periodic minimal surface structures fabricated by selective laser melting. *International Journal of Mechanical Sciences*, 204, 106586, https://doi.org/10.1016/j.ijmecsci.2021.106586

[25] Zhang, C., Zhang, H., Yang, L. (2022). Mechanical responses of sheet-based gyroid-type triply periodic minimal surface lattice structures fabricated using selective laser melting. *Materials & Design*, 214, 110407, https://doi.org/10.1016/j.matdes.2022.110407

[26] Zhang, C., Jiang, Z. L., Zhao, L. (2021). Mechanical characteristics and deformation mechanism of functionally graded triply periodic minimal surface structures fabricated using stereolithography. *International Journal of Mechanical Sciences*, 208, 106679, https://doi.org/10.1016/j.ijmecsci.2021.106679

[27] Ma, Z., Zhang, D. Z., Liu, F. (2020). Lattice structures of Cu-Cr-Zr copper alloy by selective laser melting: Microstructures, mechanical properties and energy absorption. *Materials & Design*, 187, 108406, https://doi.org/10.1016/j.matdes.2019.108406

[28] Wang, H., Su, M. M., Hao, H. (2021). Compressive properties and energy absorption behavior of Mg17Al12/Al ordered structure composites. *Composites Part B: Engineering*, 210, 108688, https://doi.org/10.1016/j.compositesb.2021.108688

[29] Zhao, M., Zhang, D. Z., Liu, F. (2020). Mechanical and energy absorption characteristics of additively manufactured functionally graded sheet lattice structures with minimal surfaces. *International Journal of Mechanical Sciences*, 167, 105262, https://doi.org/10.1016/j.ijmecsci.2019.105262

Int. Journal of Integrated Engineering Vol. 17 No. 5 (2025) p. 87-97

[30] Li, Y., Wang, X., Zhang, J. (2021). Compression behavior of triply periodic minimal surface polymer lattice structures. *Polymer Testing*, 98, 107108, https://doi.org/10.1007/s11340-023-00940-3